

A description of the transverse momentum distributions of charged particles produced in heavy ion collisions at RHIC and LHC energies

Jia-Qi Hui, Zhi-Jin Jiang*, and Dong-Fang Xu

College of Science, University of Shanghai for Science and Technology, Shanghai 200093, China

*jzj265@163.com

By assuming the existing of memory effects and long-range interactions in the hot and dense matter produced in high energy heavy ion collisions, the nonextensive statistics together with the relativistic hydrodynamics including phase transition is used to discuss the transverse momentum distributions of charged particles produced in heavy ion collisions. It is shown that the combined contributions from nonextensive statistics and hydrodynamics can give a good description to the experimental data in Au+Au collisions at $\sqrt{s_{NN}} = 200$ GeV and in Pb+Pb collisions at $\sqrt{s_{NN}} = 2.76$ TeV for π^\pm , K^\pm in the whole measured transverse momentum region, and for $p(\bar{p})$ in the region of $p_T \leq 2.0$ GeV/c. This is different from our previous work, where, by using the conventional statistics plus hydrodynamics, the describable region is only limited in $p_T \leq 1.1$ GeV/c.

Keywords: Nonextensive statistics; relativistic hydrodynamics; phase transition; transverse momentum distribution

PACS Number(s): 25.75.Ag, 25.75.Ld, 25.75.Dw, 13.85.-t

1. Introduction

The primary goals of experimental programs performed in high energy heavy ion collisions are to find the deconfined nuclear matter, namely the quark-gluon plasma (QGP), which is believed to have filled in the early universe several microseconds after the big bang. Therefore, studying the properties of QGP is important for both particle physics and cosmology. In the past decade, a number of bulk observables about charged particles, such as the Fourier coefficients v_n of azimuth-angle distributions [1, 2], transverse momentum spectra [3-8] and pseudorapidity

distributions [9-12], have been extensively studied in nuclear collisions at both RHIC and LHC energies. These investigations have shown a fact that the matter created in these collisions is in the state of strongly coupled quark-gluon plasma (sQGP) exhibiting a clear collective behavior nearly like a perfect fluid with very low viscosity [13-31]. Therefore, the movement of sQGP can be described in the scope of relativistic hydrodynamics which connects the static aspects of sQGP and the dynamical aspects of heavy ion collisions [32].

In our previous work [33], by considering the effects of thermalization, we once used a hydrodynamic model incorporating phase transition in analyzing the transverse momentum distributions of identified charged particles produced in heavy ion collisions. In that model, the quanta of hot and dense matter are supposed to observe the standard statistical distributions and the experimental measurements in Au+Au collisions at $\sqrt{s_{NN}} = 200$ and 130 GeV can be well matched up in the region of $p_T \leq 1.1$ GeV/c. Known from the investigations in Ref. [34, 35], the memory effects and long-range force might appear in the hot and dense matter. This guarantees, at least to a certain extent, the reasonableness of nonextensive statistical approach in describing the thermal motions of quanta of hot and dense matter. Hence, in this paper, on the basis of hydrodynamics taking phase transition into considerations, we will use nonextensive statistics instead of conventional statistics to simulate the transverse collective flow of the matter created in collisions.

The nonextensive statistics is also known as Tsallis nonextensive thermostatics, which was first proposed by C. Tsallis in 1988 in his pioneering work [36]. This statistical theory overcomes the shortcomings of the conventional statistics in many physical problems with long-range interactions, long-range microscopic memory, or fractal space-time constrains. It has a wide range of applications in astrophysical self-gravitating systems [37], cosmology [38], the solar neutrino problem [39], many-body theory, dynamical linear response theory and variational methods [40].

In the following section 2, a brief description is given to the adopted hydrodynamics, presenting its analytical solutions. The solutions are then used in section 3 to formulate the transverse momentum distributions of charged particles produced in heavy ion collisions in the light of nonextensive statistics and Cooper-Frye prescription. The last section 4 is about conclusions.

2. A brief introduction to the hydrodynamic model

The key points of the hydrodynamic model [18] used in the present paper are as follows.

The expansions of fluid follow the continuity equation

$$\frac{\partial T^{\mu\nu}}{\partial x^\nu} = 0, \quad \mu, \nu = 0, 1, \quad (1)$$

where $x^\nu = (x^0, x^1) = (t, z)$, and

$$T^{\mu\nu} = (\varepsilon + p)u^\mu u^\nu - pg^{\mu\nu}, \quad (2)$$

is the energy-momentum tensor of perfect fluid, where $g^{\mu\nu} = \text{diag}(1, -1)$ is the metric tensor, $u^\mu = (u^0, u^1) = (\cosh y_F, \sinh y_F)$ is the four-velocity of fluid with rapidity y_F . ε and p are the energy density and pressure of fluid, which are related by the sound speed of fluid c_s via the equation of state

$$\frac{dp}{d\varepsilon} = \frac{s dT}{T ds} = c_s^2, \quad (3)$$

where, T is the temperature, and s is the entropy density of fluid.

Project Eq. (1) to the direction of u_μ giving

$$\frac{\partial(su^\nu)}{\partial x^\nu} = 0, \quad (4)$$

which is the continuity equation for entropy conservation. Project Eq. (1) to the direction perpendicular to u_μ leading to equation

$$\frac{\partial(T \sinh y_F)}{\partial t} + \frac{\partial(T \cosh y_F)}{\partial z} = 0, \quad (5)$$

which means the existence of scalar function ϕ satisfying

$$\frac{\partial\phi}{\partial t} = T \cosh y_F, \quad \frac{\partial\phi}{\partial z} = -T \sinh y_F. \quad (6)$$

From ϕ and Legendre transformation, Khalatnikov potential χ is introduced by

$$\chi = \phi - tT \cosh y_F + zT \sinh y_F, \quad (7)$$

which makes the coordinates of (t, z) transform to

$$t = \frac{e^\omega}{T_0} \left(\frac{\partial\chi}{\partial\omega} \cosh y_F + \frac{\partial\chi}{\partial y_F} \sinh y_F \right), \quad (8)$$

$$z = \frac{e^\omega}{T_0} \left(\frac{\partial\chi}{\partial\omega} \sinh y_F + \frac{\partial\chi}{\partial y_F} \cosh y_F \right), \quad (9)$$

where T_0 is the initial temperature of fluid, and $\omega = \ln(T_0 / T)$. In terms of χ , Eq. (4) can be rewritten as the so-called telegraphy equation

$$\frac{\partial^2 \chi}{\partial \omega^2} - 2\beta \frac{\partial \chi}{\partial \omega} - \frac{1}{c_s^2} \frac{\partial^2 \chi}{\partial y_F^2} = 0, \quad \beta = \frac{1-c_s^2}{2c_s^2}. \quad (10)$$

With the expansions of created matter, its temperature becomes lower and lower. When the temperature reduces from initial temperature T_0 to critical temperature T_c , the matter transforms from the sQGP state to the hadronic state. The produced hadrons are initially in the violent and frequent collisions, which are mainly inelastic. Hence, the abundance of identified hadrons is in changing. Furthermore, the mean free paths of these primary hadrons are very short. The evolution of them still satisfies Eq. (10) with only difference being the values of c_s . In sQGP, $c_s = c_0 = 1/\sqrt{3}$. In the hadronic state, $0 < c_s = c_h \leq c_0$. At the point of phase transition, c_s is discontinuous.

The solutions of Eq. (10) for the sQGP and hadronic state are respectively [18],

$$\chi_0(\omega, y_F) = \frac{Q_0 c_0}{2} e^{\beta_0 \omega} I_0 \left(\beta_0 \sqrt{\omega^2 - c_0^2 y_F^2} \right), \quad (11)$$

$$\chi_h(\omega, y_F) = \frac{Q_0 c_0}{2} S(\omega) I_0 [\lambda(\omega, y_F)], \quad (12)$$

where Q_0 is a constant determined by fitting the theoretical results with experimental data, I_0 is the 0th order modified Bessel function, and

$$\begin{aligned} \beta_0 &= (1 - c_0^2) / 2c_0^2 = 1, \quad S(\omega) = e^{\beta_h(\omega - \omega_c) + \beta_0 \omega_c}, \quad \lambda(\omega, y_F) = \beta_h c_h \sqrt{y_h^2(\omega) - y_F^2}, \\ \beta_h &= (1 - c_h^2) / 2c_h^2, \quad \omega_c = \ln(T_0 / T_c), \quad y_h(\omega) = [(\omega - \omega_c) / c_h] + (\omega_c / c_0). \end{aligned}$$

3. The transverse momentum distributions of charged particles produced in heavy ion collisions

(1) The energy of quantum of produced matter

In the nonextensive statistics, there are two basic postulations [36, 39]

(a) The entropy of a statistical system possesses the form of

$$s_q = \frac{1}{q-1} \sum_{i=1}^{\Omega} p_i (1 - p_i^{q-1}), \quad (13)$$

where p_i is the probability of a given microstate among Ω different ones and q is a real parameter.

(b) The mean value of an observable O is given by

$$\bar{O}_q = \sum_{i=1}^{\Omega} p_i^q O_i, \quad (14)$$

where O_i is the value of an observable O in the microstate i .

From above two postulations, the average occupational number of quantum in the state with

temperature T can be written in a simple analytical form [41]

$$\bar{n}_q = \frac{1}{[1+(q-1)(E-\mu_B)/T]^{1/(q-1)+\delta}}, \quad (15)$$

where, E is the energy of quantum, and μ_B is its baryochemical potential. $\delta = 1$ for fermions, and $\delta = -1$ for Bosons. In the limit of $q \rightarrow 1$, it reduces to the conventional Fermi-Dirac or Bose-Einstein distributions. Hence, the value of q reflects the discrepancies of nonextensive statistics from conventional one. Known from Eq. (15), the average energy of quantum in the state with temperature T reads

$$\bar{E}_q = \frac{m_T \cosh(y-y_F)}{\{1+[(q-1)(m_T \cosh(y-y_F)-\mu_B)]/T\}^{1/(q-1)+\delta}}, \quad (16)$$

where, y is the rapidity of quantum, $m_T = \sqrt{p_T^2 + m^2}$ is its transverse mass with rest mass m and transverse momentum p_T .

(2) The rapidity distributions of charged particles in the state of fluid

In terms of Khalatnikov potential χ , the rapidity distributions of charged particles in the state of fluid can be written as [42]

$$\frac{dN}{dy_F} = \frac{Q_0 c_0}{2} A(b) \left(\cosh y \frac{dz}{dy_F} - \sinh y \frac{dt}{dy_F} \right), \quad (17)$$

where

$$A(b) = 2r^2 \arccos \frac{b}{2r} - b \sqrt{r^2 - \left(\frac{b}{2}\right)^2}$$

is the area of overlap region of collisions, b is impact parameter, and r is the radius of colliding nucleus. From Eqs. (8) and (9), the expression in the round brackets in Eq. (17) becomes

$$\begin{aligned} & \cosh y \frac{dz}{dy_F} - \sinh y \frac{dt}{dy_F} \\ &= \frac{1}{T} c_s^2 \frac{\partial}{\partial \omega} \left(\chi + \frac{\partial \chi}{\partial \omega} \right) \cosh(y - y_F) - \frac{1}{T} \frac{\partial}{\partial y_F} \left(\chi + \frac{\partial \chi}{\partial \omega} \right) \sinh(y - y_F). \end{aligned} \quad (18)$$

(3) The transverse momentum distributions of charged particles produced in heavy ion collisions

Along with the expansions of hadronic matter, its temperature becomes even lower. As the temperature drops to kinetic freeze-out temperature T_f , the inelastic collisions among hadronic matter stop. The yields of identified hadrons keep unchanged becoming the measured results. According to Cooper-Frye scheme [42], the invariant multiplicity distributions of charged particles take the form as [18, 42, 43]

$$\frac{d^2N}{2\pi p_T dy dp_T} = \frac{1}{(2\pi)^3} \int_{-y_h(\omega_f)}^{y_h(\omega_f)} \left(\frac{dN}{dy_F} \times \bar{E}_q \right) \Big|_{T=T_f} dy_F, \quad (19)$$

where $\omega_f = \ln(T_0 / T_f)$, and the integrand takes values at the moment of $T = T_f$. Substituting χ in Eq. (18) by the χ_h of Eq. (12), it becomes

$$\begin{aligned} & \left(\cosh y \frac{dz}{dy_F} - \sinh y \frac{dt}{dy_F} \right) \Big|_{T=T_f} \\ &= \frac{1}{T_f} (\beta_h c_h)^2 S(\omega_f) [B(\omega_f, y_F) \sinh(y - y_F) + C(\omega_f, y_F) \cosh(y - y_F)], \end{aligned} \quad (20)$$

where

$$B(\omega_f, y_F) = \frac{\beta_h y_F}{\lambda(\omega_f, y_F)} \left\{ \frac{\beta_h c_h y_h(\omega_f)}{\lambda(\omega_f, y_F)} I_0[\lambda(\omega_f, y_F)] + \left[\frac{\beta_h + 1}{\beta_h} - \frac{2\beta_h c_h y_h(\omega_f)}{\lambda^2(\omega_f, y_F)} \right] I_1[\lambda(\omega_f, y_F)] \right\}, \quad (21)$$

$$\begin{aligned} C(\omega_f, y_F) &= \left\{ \frac{\beta_h + 1}{\beta_h} + \frac{[\beta_h c_h y_h(\omega_f)]^2}{\lambda^2(\omega_f, y_F)} \right\} I_0[\lambda(\omega_f, y_F)] \\ &+ \frac{1}{\lambda(\omega_f, y_F)} \left\{ \frac{y_h(\omega_f)}{c_h} + 1 - \frac{2[\beta_h c_h y_h(\omega_f)]^2}{\lambda^2(\omega_f, y_F)} \right\} I_1[\lambda(\omega_f, y_F)] \end{aligned} \quad (22)$$

where I_1 is the 1st order modified Bessel function.

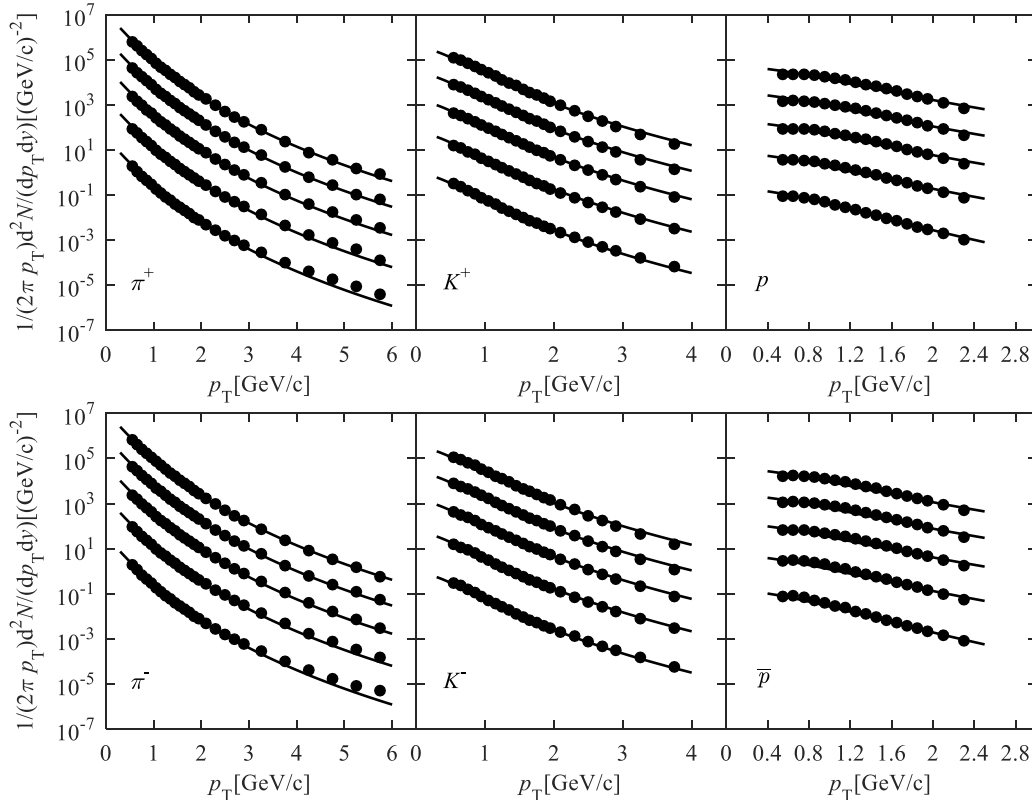


FIGURE 1: The invariant yields of π^\pm , K^\pm , and $p(\bar{p})$ as a function of p_T in Au+Au collisions at $\sqrt{s_{NN}} = 200$ GeV. The solid dots represent the experimental data of the PHENIX Collaboration [3]. The solid curves are the results calculated from Eq. (19). The centrality cuts counted from top to bottom in each panel are 0-10% ($\times 10^4$), 10-20% ($\times 10^3$), 20-40% ($\times 10^2$), 40-60% ($\times 10^1$), 60-92% ($\times 10^0$), respectively.

By using Eqs. (17) and (19)-(22), we can obtain the transverse momentum distributions of identified charged particles as shown in figures 1 and 2.

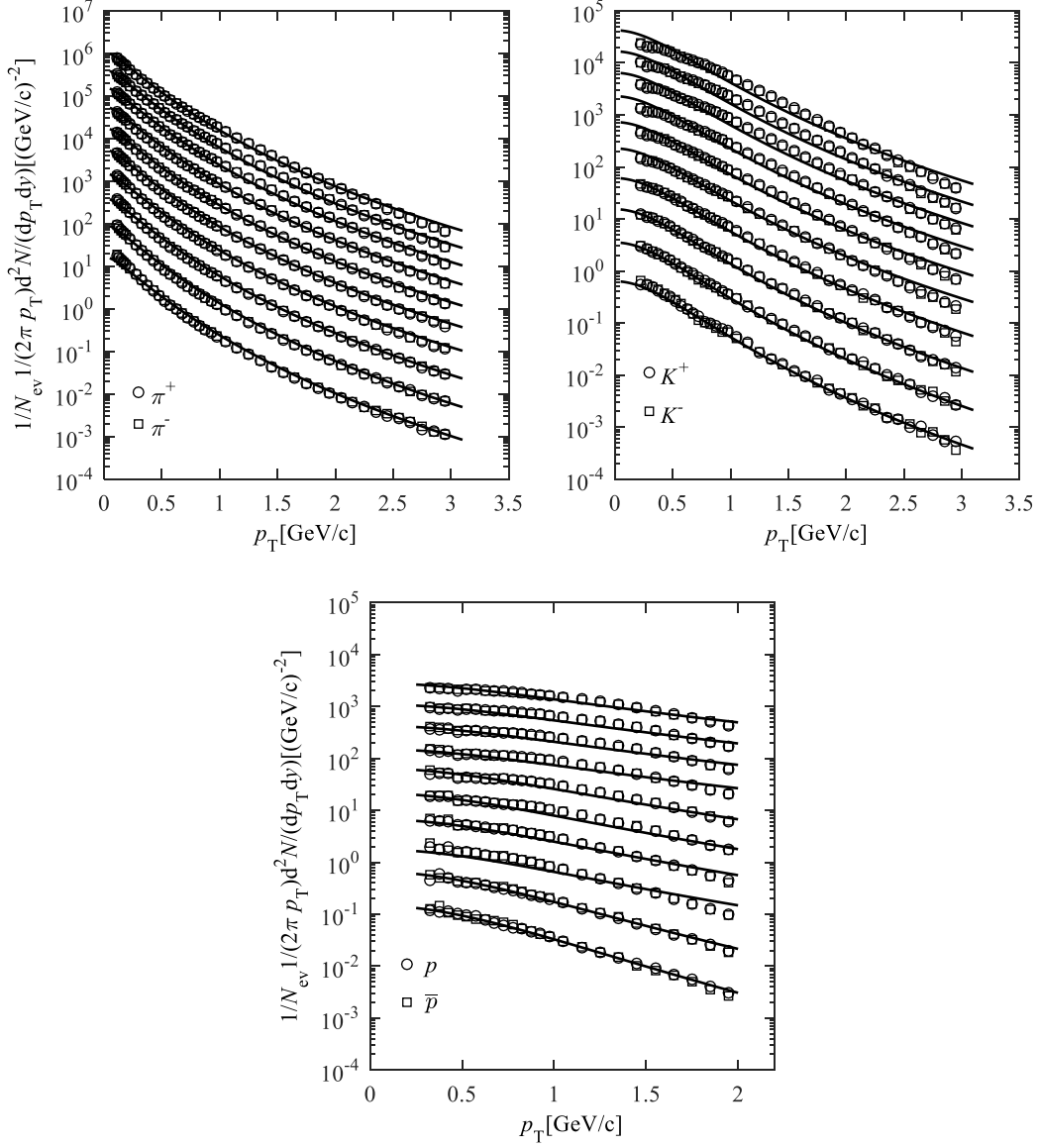


FIGURE 2: The invariant yields of π^\pm , K^\pm , and $p(\bar{p})$ as a function of p_T in Pb+Pb collisions at $\sqrt{s_{NN}} = 2.76$ TeV. The circles and squares represent the experimental data of the ALICE Collaboration [4]. The solid curves are the results calculated from Eq. (19). The centrality cuts counted from top to bottom in each panel are 0-5% ($\times 2^9$), 5-10% ($\times 2^8$), 10-20% ($\times 2^7$), 20-30% ($\times 2^6$), 30-40% ($\times 2^5$), 40-50% ($\times 2^4$), 50-60% ($\times 2^3$), 60-70% ($\times 2^2$), 70-80% ($\times 2^1$), and 80-90% ($\times 2^0$), respectively.

Figure 1 shows the invariant yields of π^\pm , K^\pm , and $p(\bar{p})$ as a function of p_T in Au+Au collisions at $\sqrt{s_{NN}} = 200$ GeV. Figure 2 shows the same distributions in Pb+Pb collisions at $\sqrt{s_{NN}} = 2.76$ TeV. The solid dots represent the experimental data [3, 4]. The solid curves are the

results calculated from Eq. (19). It can be seen that the theoretical results are in good agreement with the experimental data for π^\pm , K^\pm in the whole measured p_T region. For $p(\bar{p})$, the theoretical model works well in the region up to about $p_T \leq 2.0$ GeV/c. Beyond this region, the deviation appears as shown in figure 3, which presents the fittings for $p(\bar{p})$ in both the most peripheral collisions for p_T up to about 4 GeV/c.

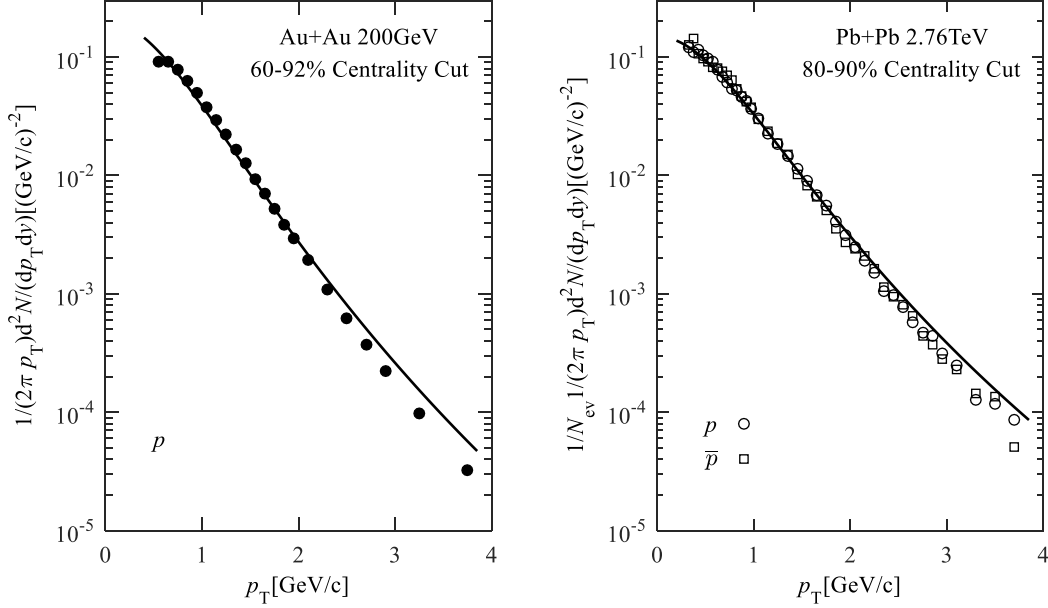


FIGURE 3: The invariant yields of $p(\bar{p})$ as a function of p_T in 60-92% Au+Au collisions at $\sqrt{s_{NN}} = 200$ GeV (left panel) and in 80-90% Pb+Pb collisions at $\sqrt{s_{NN}} = 2.76$ TeV (right panel). The meanings of solid dots, circles, squares, and solid curves are the same as those in figures 1 and 2.

In analyses, the sound speed in hadronic state takes the value of $c_h = 0.35$ [43, 44-46]. The critical temperature takes the value of $T_c = 0.18$ GeV [47]. The kinetic freeze-out temperature T_f takes the values of 0.12 GeV for pions, kaons and 0.13 GeV for protons, respectively, from the investigations of Ref. [8], which also shows that the baryochemical potential μ_B is about 0.019 GeV in Au+Au collisions. For Pb+Pb collisions, μ_B takes the value of $\mu_B = 0$ owing to the fact that the yields of particles and antiparticles are equal in such collisions [4]. The initial temperature in central Au+Au collisions takes the same value of $T_0 = 0.7$ GeV as that used in Ref. [43]. For central Pb+Pb collisions, T_0 takes the value of $T_0 = 6.5$ GeV referring to that used in Ref. [48]. Tables 1 and 2 list the values of T_0 , q and Q_0 in different centrality cuts. It can be seen that T_0 decreases with increasing centrality cuts. q is slightly larger than 1 for different kinds of charged particles. It is almost irrelevant to centrality cuts, while increases with the mass of charged particles on the whole. Q_0 is independent of centrality cuts for different kinds of charged particles in Au+Au collisions. The fitted Q_0 in table 1 gives

$$\frac{Q_0(\pi^-)}{Q_0(\pi^+)} = 1, \frac{Q_0(K^-)}{Q_0(K^+)} = 0.917, \frac{Q_0(\bar{p})}{Q_0(p)} = 0.7 \text{ (Au+Au 200 GeV)}. \quad (23)$$

These ratios are in good agreement with the relative abundances of particles and antiparticles given in Ref. [3]. This consistency may be due to the fact that the integrand of Eq. (19) is the same for particles and antiparticles in case that T_f takes a common constant for these two kinds of particles. Therefore, Q_0 might be proportional to the abundance of corresponding particles. The Q_0 in Pb+Pb collisions is also independent of centrality cuts for π^\pm and K^\pm . While for $p(\bar{p})$, Q_0 increases with centrality cuts from semicentral to peripheral collisions. The Q_0 listed in table 2 gives the ratios

$$\frac{Q_0(\pi^-)}{Q_0(\pi^+)} = \frac{Q_0(K^-)}{Q_0(K^+)} = \frac{Q_0(\bar{p})}{Q_0(p)} = 1. \quad (24)$$

This is consistent with the above stated fact that, in Pb+Pb collisions at $\sqrt{s_{NN}} = 2.76$ TeV, the yield of charged particles is equal to that of antiparticles.

TABLE 1. The values of T_0 , q , and Q_0 in different centrality Au+Au collisions at $\sqrt{s_{NN}} = 200$ GeV.

Centrality Cuts	$T_0(\text{GeV})$	$q(\pi/K/p)$	$Q_0(\pi^+/\pi^-)$	$Q_0(K^+/K^-)$	$Q_0(p/\bar{p})$
0-10%	0.70	1.08/1.01/1.12	0.070/0.070	0.024/0.022	0.020/0.014
10-20%	0.70	1.08/1.01/1.12	0.070/0.070	0.024/0.022	0.020/0.014
20-40%	0.69	1.08/1.01/1.12	0.070/0.070	0.024/0.022	0.020/0.014
40-60%	0.68	1.08/1.01/1.11	0.070/0.070	0.024/0.022	0.020/0.014
60-92%	0.67	1.08/1.09/1.09	0.070/0.070	0.024/0.022	0.020/0.014

TABLE 2: The values of T_0 , q , and Q_0 in deferent centrality Pb+Pb collisions at $\sqrt{s_{NN}} = 2.76$ TeV

Centrality Cuts	$T_0(\text{GeV})$	$q(\pi/K/p)$	$Q_0(\times 10^4) (\pi^+/\pi^-)$	$Q_0(\times 10^4) (K^+/K^-)$	$Q_0(\times 10^4) (p/\bar{p})$
0-5%	6.5	1.11/1.13/1.26	0.750/0.750	0.200/0.200	0.025/0.025
5-10%	6.4	1.11/1.13/1.26	0.750/0.750	0.200/0.200	0.025/0.025
10-20%	6.2	1.11/1.13/1.26	0.750/0.750	0.200/0.200	0.025/0.025
20-30%	5.9	1.11/1.13/1.26	0.750/0.750	0.200/0.200	0.025/0.025
30-40%	5.4	1.11/1.13/1.20	0.750/0.750	0.200/0.200	0.060/0.060
40-50%	4.9	1.11/1.13/1.18	0.750/0.750	0.200/0.200	0.080/0.080
50-60%	4.3	1.11/1.13/1.18	0.750/0.750	0.200/0.200	0.090/0.090
60-70%	3.7	1.11/1.12/1.18	0.750/0.750	0.200/0.200	0.090/0.090
70-80%	3.1	1.11/1.11/1.12	0.750/0.750	0.200/0.200	0.300/0.300
80-90%	2.4	1.10/1.11/1.10	0.750/0.750	0.200/0.200	0.500/0.500

4. Conclusions

By introducing nonextensive statistics, we employ the relativistic hydrodynamics including phase transition to discuss the transverse momentum distributions of charged particles produced in Au+Au collisions at $\sqrt{s_{NN}} = 200$ GeV and in Pb+Pb collisions at $\sqrt{s_{NN}} = 2.76$ TeV. The model contains a rich information about the transport coefficients of fluid, such as the initial temperature T_0 , the critical temperature T_c , the kinetic freeze-out temperature T_f , the baryochemical potential μ_B , the sound speed in sQGP state c_0 and the sound speed in hadronic state c_h . Except for T_0 , the other five parameters take the values either from widely accepted theoretical results or from experimental measurements. As for T_0 , there are no acknowledged values so far. In this paper, T_0 takes the values from other studies for the most central collisions, and for the rest centrality cuts, T_0 is determined by tuning the theoretical results to experimental data. The present investigations show the conclusions as follows:

(1) The theoretical model can give a good description to the experimental data in Au+Au collisions at $\sqrt{s_{NN}} = 200$ GeV and in Pb+Pb collisions at $\sqrt{s_{NN}} = 2.76$ TeV for π^\pm , K^\pm in the whole measured transverse momentum region, and for $p(\vec{p})$ in the region of $p_T \leq 2.0$ GeV/c.

(2) The fitted q is close to 1. It might mean that the difference between nonextensive statistics and conventional statistics is small. However, it is this small difference that plays an essential role in extending the fitting region of p_T .

(3) Q_0 is independent of centrality cuts for different charged particles in Au+Au collisions at $\sqrt{s_{NN}} = 200$ GeV. For Pb+Pb collisions, Q_0 is irrelevant to centrality cuts for π^\pm and K^\pm , while increases from semicentral to peripheral collisions for $p(\vec{p})$.

(4) The methods cannot describe the experimental measurements for $p(\vec{p})$ in the region of $p_T \geq 2.0$ GeV/c for the both kinds of collisions. This might be caused by the hard scattering process [49]. To improve the fitting conditions, the results from perturbative QCD should be taken into account.

Conflict of Interests

The authors declare that there is no conflict of interests regarding the publication of this paper.

Acknowledgments

This work is supported by the Shanghai Key Lab of Modern Optical System.

References

- [1] L. Adamczyk and STAR Collaboration, “Centrality dependence of identified particle elliptic flow in relativistic heavy ion collisions at $\sqrt{s_{NN}} = 7.7\text{-}62.4$ GeV,” *Physical Review C*, vol. 93, Article ID 014907, 2016.
- [2] J. Adam and ALICE Collaboration, “Anisotropic Flow of Charged Particles in Pb-Pb Collisions at $\sqrt{s_{NN}} = 5.02$ TeV,” *Physical Review Letters*, vol. 116, Article ID 132302, 2016.
- [3] A. Adare and PHENIX Collaboration, “Spectra and ratios of identified particles in Au+Au and d+Au collisions at $\sqrt{s_{NN}} = 200$ GeV,” *Physical Review C*, vol. 88, Article ID 024906, 2013.
- [4] B. Abelev and ALICE Collaboration, “Centrality dependence of π , K , and p production in Pb-Pb collisions at $\sqrt{s_{NN}} = 2.76$ TeV,” *Physical Review C*, vol. 88, Article ID 044910, 2013.
- [5] K. Adcox and PHENIX Collaboration, “Single identified hadron spectra from $\sqrt{s_{NN}} = 130\text{GeV}$ Au+Au collisions,” *Physical Review C*, vol. 69, Article ID 024904, 2004.
- [6] C. Adler and STAR Collaboration, “Measurement of Inclusive Antiprotons from Au+Au Collisions at $\sqrt{s_{NN}} = 130$ GeV,” *Physical Review Letters*, vol. 87, Article ID 262302, 2001.
- [7] K. Adcox and PHENIX Collaboration, “Centrality Dependence of π^\pm , K^\pm , p , and \bar{p} Production from $\sqrt{s_{NN}} = 130$ GeV Au+Au Collisions at RHIC,” *Physical Review Letters*, vol. 88, Article ID 242301, 2002.
- [8] B. I. Abelev and STAR Collaboration, “Systematic measurements of identified particle spectra in pp , d+Au, and Au+Au collisions at the STAR detector,” *Physical Review C*, vol. 79, Article ID 034909, 2009.
- [9] B. Alver and PHOBOS Collaboration, “Charged-particle multiplicity and pseudorapidity distributions measured with the PHOBOS detector in Au+Au, Cu+Cu, d+Au, and $p+p$ collisions at ultrarelativistic energies,” *Physical Review C*, vol. 83, Article ID 024913, 2011.
- [10] M. Murray (for the BRAHMS Collaboration), “Scanning the phases of QCD with BRAHMS,” *Journal of Physics G: Nuclear and Particle Physics*, vol. 30, pp. 667-674, 2004.
- [11] M. Murray (for the BRAHMS Collaboration), “Flavor dynamics,” *Journal of Physics G: Nuclear and Particle Physics*, vol. 35, Article ID 044015, 2008.
- [12] I. G. Bearden and BRAHMS Collaboration, “Charged Meson Rapidity Distributions in Central Au+Au Collisions at $\sqrt{s_{NN}} = 200$ GeV,” *Physical Review Letters*, vol. 94, Article ID 162301, 2005.
- [13] A. Bialas, R. A. Janik and R. Peschanski, “Unified description of Bjorken and Landau 1+1 hydrodynamics,” *Physical Review C*, vol. 76, Article ID 054901, 2007.
- [14] C. Y. Wong, “Landau hydrodynamics reexamined,” *Physical Review C*, vol. 78, Article ID 054902, 2008.
- [15] G. Beuf, R. Peschanski and E. N. Saridakis, “Entropy flow of a perfect fluid in (1+1) hydrodynamics,”

Physical Review C, vol. 78, Article ID 064909, 2008.

- [16] T. Csörgő, M. I. Nagy and M. Csanád, “New family of simple solutions of relativistic perfect fluid Hydrodynamics,” *Physical Review B*, vol. 663, pp. 306-311, 2008.
- [17] Z. W. Wang, Z. J. Jiang and Y. S. Zhang, “The investigations of pseudorapidity distributions of final multiplicity in Au+Au collisions at high energy,” *Journal of university of Shanghai for science and technology*, vol. 31, pp. 322-326, 2009. (in Chinese)
- [18] N. Suzuki, “One-dimensional hydrodynamical model including phase transition,” *Physical Review C*, vol. 81, Article ID 044911, 2010.
- [19] E. K. G. Sarkisyan and A. S. Sakharov, “Relating multihadron production in hadronic and nuclear collisions,” *European Physical Journal C*, vol. 70, pp. 533-541, 2010.
- [20] A. Bialas and R. Peschanski, “Asymmetric (1+1)-dimensional hydrodynamics in high-energy collisions,” *Physical Review C*, vol. 83, Article ID 054905, 2011.
- [21] M. Csanád, M. I. Nagy and S. Lökös, “Exact solutions of relativistic perfect fluid hydrodynamics for a QCD Equation of State,” *The European Physical Journal A*, vol. 48, pp. 173-178, 2012.
- [22] Z. J. Jiang, Q. G. Li and H. L. Zhang, “Revised Landau hydrodynamic model and the pseudorapidity distributions of charged particles produced in nucleus-nucleus collisions at maximum energy at the BNL Relativistic Heavy Ion Collider,” *Physical Review C*, vol. 87, Article ID 044902, 2013.
- [23] C. Gale, S. Jeon and B. Schenke, “Hydrodynamic modeling of heavy-ion collisions,” *International Journal of Modern Physics A*, vol. 28, Article ID 1340011, 2013.
- [24] U. Heinz and R. Snellings, “Collective flow and viscosity in relativistic heavy-ion collisions,” *Annual Review of Nuclear and Particle Science*, vol. 63, pp. 123-151, 2013.
- [25] A. N. Mishra, R. Sahoo, E. K. G. Sarkisyan and A. S. Sakharov, “Effective-energy budget in multiparticle production in nuclear collisions,” *The European Physical Journal C*, vol. 74, p. 3147, 2014.
- [26] Z. J. Jiang, Y. Zhang, H. L. Zhang and H. P. Deng, “A description of the pseudorapidity distributions in heavy ion collisions at RHIC and LHC energies,” *Nuclear Physics A*, vol. 941, pp. 188-200, 2015.
- [27] H. Niemi, K. J. Eskola and R. Paatelainen, “Event-by-event fluctuations in a perturbative QCD+saturation+hydrodynamics model: Determining QCD matter shear viscosity in ultrarelativistic heavy-ion collisions,” *Physical Review C*, vol. 93, Article ID 024907, 2016.
- [28] J. Noronha-Hostler, M. Luzum and J. Y. Ollitrault, “Hydrodynamic predictions for 5.02 TeV Pb-Pb Collisions,” *Physical Review C-Nuclear Physics*, vol. 93, Article ID 034912, 2016.

- [29] J. S. Moreland and R. A. Soltz, “Hydrodynamic simulations of relativistic heavy-ion collisions with different lattice quantum chromodynamics calculations of the equation of state,” *Physical Review C*, vol. 93, Article ID 044913, 2016.
- [30] E. K. G. Sarkisyan, A. N. Mishra, R. Sahoo and A. S. Sakharov, “Multihadron production dynamics exploring the energy balance in hadronic and nuclear collisions,” *Physical Review D*, vol. 93, Article ID 054046, 2016.
- [31] E. K. G. Sarkisyan, A. N. Mishra, R. Sahoo and A. S. Sakharov, “Centrality dependence of midrapidity density from GeV to TeV heavy-ion collisions in the effective-energy universality picture of hadroproduction,” *Physical Review D*, vol. 94, Article ID 011501, 2016.
- [32] T. Hirano, N. van der Kolk, and A. Bilandzic, “Hydrodynamics and Flow,” *Lecture Notes in Physics*, vol. 785, pp. 139-178, 2008.
- [33] Z. J. Jiang, J. Q. Hui and Y. Zhang, “The rapidity distributions and the thermalization induced transverse momentum distributions in Au-Au collisions at RHIC energies,” *Advances in High Energy Physics*, vol. 2017, Article ID 6896524, 2017.
- [34] W. M. Alberico, A. Lavagno and P. Quarati, “Nonextensive statistics, fluctuations and correlations in high energy nuclear collisions,” *The European Physical Journal C*, vol. 13, pp. 499-506, 2000.
- [35] M. Biyajima, T. Mizoguchi, N. Nakajima, N. Suzuki and G. Wilk, “Modified Hagedorn formula including temperature fluctuation: Estimation of temperatures at RHIC experiments,” *The European Physical Journal C*, vol. 48, pp. 597-603, 2006.
- [36] C. Tsallis, “Possible Generalization of Boltzmann-Gibbs Statistics,” *Journal of Statistical Physics*, vol. 52, pp. 479-487, 1988.
- [37] A. R. Plastino and A. Plastino, “Information theory, approximate time dependent solutions of Boltzmann’s equation and Tsallis’ entropy,” *Physics Letters A*, vol. 193, pp. 251-258, 1994.
- [38] D. F. Torres, H. Vucetich and P. Plastino, “Early Universe Test of Nonextensive Statistics,” *Physical Review Letters*, vol. 79, pp. 1588-1590, 1997.
- [39] G. Kaniadakis, A. Lavagno, M. Lissia and P. Quarati, “Nonextensive statistical effects in nuclear physics problems,” *Physica A*, vol. 261, p. 359, 1998.
- [40] A. K. Rajagopal, R. Mendes and E. K. Lenzi, “Quantum Statistical Mechanics for Nonextensive Systems: Prediction for Possible Experimental Tests,” *Physical Review Letters*, vol. 80, p. 3907, 1998.
- [41] U. Tirnakli, F. Büyükkiliç, D. Demirhan, “Some bounds upon the nonextensivity parameter using the approximate generalized distribution functions,” *Physics Letters A*, vol. 245, pp. 62-66, 1998.

- [42] F. Cooper and G. Frye, “Landau’s hydrodynamic model of particle production and electron-positron annihilation into hadrons,” *Physical Review D*, vol. 11, pp. 192-213, 1975.
- [43] T. Mizoguchi, H. Miyazawa and M. Biyajima, “A potential including the Heaviside function in the 1+1 dimensional hydrodynamics by Landau: Its basic properties and application to data at RHIC energies,” *The European Physical Journal A*, vol. 40, pp. 99-108, 2009.
- [44] A. Adare and PHENIX Collaboration, “Scaling properties of azimuthal anisotropy in Au+Au and Cu+Cu collisions at $\sqrt{s_{NN}} = 200$ GeV,” *Physical Review Letters*, vol. 98, Article ID 162301, 2007.
- [45] L. N. Gao, Y. H. Chen, H. R. Wei, and F. H. Liu, “Speed of sound parameter from RHIC and LHC heavy-ion Data,” *Advances in High Energy Physics*, vol. 2014, Article ID 450247, 2014.
- [46] S. Borsányi, G. Endrődi, Z. Fodor, A. Jakovác, S. D. Katz, S. Krieg, C. Ratti and K. K. Szabó, “The QCD equation of state with dynamical quarks,” *Journal of High Energy Physics*, vol. 2010, pp. 1-31, 2010.
- [47] E. Laermann and O. Philipsen, “The Status of Lattice QCD at Finite Temperature,” *Annual Review of Nuclear & Particle Science*, vol. 53, pp. 163-198, 2003.
- [48] Z. J. Jiang, J. Q. Hui and Y. Zhang, “A hydrodynamic model including phase transition and the thermal motion-induced transverse momentum distributions in high energy ion collisions,” *International Journal of Modern Physics E*, vol. 26, Article ID 1750045, 2017.
- [49] H. L. Lao, F. H. Liu, and R. A. Lacey, “Extracting kinetic freeze-out temperature and radial flow velocity from an improved Tsallis distribution,” *The European Physical Journal A*, vol. 53, pp. 44-64, 2017.